Climatic Change (2013) 116:547–563
DOI 10.1007/s10584-012-0510-9

Assessing vulnerability due to sea-level rise in Maui, Hawai'i using LiDAR remote sensing and GIS

Hannah M. Cooper · Qi Chen · Charles H. Fletcher · Matthew M. Barbee

Received: 19 September 2011 / Accepted: 22 May 2012 / Published online: 15 June 2012

Abstract Sea-level rise (SLR) threatens islands and coastal communities due to vulnerable infrastructure and populations concentrated in low-lying areas. LiDAR (Light Detection and Ranging) data were used to produce high-resolution DEMs (Digital Elevation Model) for Kahului and Lahaina, Maui, to assess the potential impacts of future SLR. Two existing LiDAR datasets from USACE (U.S. Army Corps of Engineers) and NOAA (National Oceanic and Atmospheric Administration) were compared and calibrated using the Kahului Harbor tide station. Using tidal benchmarks is a valuable approach for referencing LiDAR in areas lacking an established vertical datum, such as in Hawai'i and other Pacific Islands. Exploratory analysis of the USACE LiDAR ground returns (point data classified as ground after the removal of vegetation and buildings) indicated that another round of filtering could reduce commission errors. Two SLR scenarios of 0.75 (best-case) to 1.9 m (worst-case) (Vermeer and Rahmstorf Proc Natl Acad Sci 106:21527–21532, 2009) were considered, and the DEMs were used to identify areas vulnerable to flooding. Our results indicate that if no adaptive strategies are taken, a loss ranging from $18.7 million under the best-case SLR scenario to $296 million under the worst-case SLR scenario for Hydrologically Connected (HC; marine inundation) and Hydrologically Disconnected (HD; drainage problems due to a higher water table) areas combined is possible for Kahului; a loss ranging from $57.5 million under the best-case SLR scenario to $394 million under the worst-case SLR scenario for HC

H. M. Cooper (✉) · Q. Chen
Department of Geography, University of Hawai'i, 2424 Maile Way, Honolulu, HI 96822, USA
e-mail: hannahco@hawaii.edu

Q. Chen
e-mail: qichen@hawaii.edu

H. M. Cooper · C. H. Fletcher · M. M. Barbee
Department of Geology and Geophysics, School of Ocean and Earth Science and Technology, University of Hawai'i, 1680 East West Road, Honolulu, HI 96822, USA

C. H. Fletcher
e-mail: fletcher@soest.hawaii.edu

M. M. Barbee
e-mail: mbarbee@hawaii.edu

and HD areas combined is possible for Lahaina towards the end of the century. This loss would be attributable to inundation between 0.55 km^2 to 2.13 km^2 of area for Kahului, and 0.04 km^2 to 0.37 km^2 of area for Lahaina.

1 Introduction

Accelerated sea-level rise (SLR) due to climate change threatens human communities living near the coast worldwide. It is estimated that about half of the world's population lives in coastal areas (GOF 2011). According to the U.S. Census Bureau (2011), about half of the U.S. population lives in coastal counties. As population and land development continue to grow in low-lying coastal communities, the impacts of climate change will become more apparent (CCSP 2009).

According to the Intergovernmental Panel on Climate Change (IPCC 2007), global sea level may rise 0.18 to 0.59 m by the end of the 21st century. Thermal expansion of ocean water and melting of land-based ice are the two major contributors to global SLR. However, the IPCC (2007) estimates are understood to underestimate global SLR by 2100 because they exclude important contributions due to some forms of ice melt (Fletcher 2009).

Vermeer and Rahmstorf (2009) modeled that global sea level may rise 0.75 to 1.9 m by the end of the 21st century. To estimate the overall sea level response including ice melt, they developed a semi-empirical model based on observed global sea level and temperature data from 1880–2000 to find that the rate of SLR is closely connected to global temperature. The Vermeer and Rahmstorf model was applied to the IPCC global temperature estimates for 1880–2100; they found that late in the 21st century, thermal expansion declines as ice melt begins to increase. As their model shows that ice melt will become more important later in the 21st century, Vermeer and Rahmstorf (2009) estimates of global SLR by 2100 are significantly different than IPCC (2007) estimates.

Vulnerability to SLR is a function of a community's potential exposure, sensitivity, and adaptive capacity (IPCC 2007). The major impacts of SLR on natural systems include: inundation, wetland loss, erosion, saltwater intrusion, areas of less drainage and rising water tables; as a result, this may lead to adverse socioeconomic impacts on coastal populations/infrastructure, ports/industry, recreational activities and tourism (Nicholls 2011). Vulnerability may be influenced by social factors such as population, physical factors such as infrastructure (Wu et al. 2002), and economic factors such as land and building value. Socioeconomic factors such as these determine a coastal community's vulnerability to SLR (McLeod et al. 2010). One way to assess vulnerability is to map low-lying areas utilizing a DEM (Digital Elevation Model). DEMs are critical to mapping low-lying lands and to identifying communities, infrastructure, and coastal habitats vulnerable to inundation due to SLR.

Gesch (2009) compared DEMs used in previous SLR vulnerability assessments such as U.S. Geological Survey (USGS) global 30-arc second GTOPO30 (~1 km horizontal resolution), Shuttle Radar Topographic Mission (SRTM) (~90 m horizontal resolution), and National Elevation Dataset (NED) (30 m horizontal resolution) with Light Detection and Ranging (LiDAR) (3 m horizontal resolution) to determine that LiDAR DEMs provide improvements to mapping vulnerable lands due to their high horizontal resolution and vertical accuracy. Zhang (2011) examined the effect of vertical accuracy of DEMs comparing a 30 m LiDAR DEM with a 30 m USGS

DEM to determine that the high vertical accuracy of LiDAR DEMs is essential to estimating land area, population and property vulnerable to SLR. Zhang (2011) also examined the effect of horizontal resolution on identifying individual properties vulnerable to SLR by comparing 30 and 5 m LiDAR DEMs to determine that LiDAR DEMs ≤5 m horizontal resolution are necessary. Poulter and Halpin (2008) investigated the effects of horizontal resolution and hydrologic connectivity using 15 and 6 m LiDAR DEMs to determine that the rules for hydrologic connectivity interacted with horizontal resolution most critically at SLR scenarios <0.4 m.

In Hawai‘i, high-resolution LiDAR DEMs are useful to assess the impacts of SLR. Hawai‘i is the only U.S. state that consists exclusively of islands, where socioeconomic activity is concentrated in low-lying coastal communities. Clearly, accelerated SLR may be one of the most significant impacts of climate change in the region. However, the implications of climate change on the Hawai‘i archipelago is not well understood. There is an urgent need to improve community resiliency to marine hazards, and coastal planning in Hawai‘i currently does not require SLR vulnerability assessments to help planners identify the lowest-lying lands and the critical infrastructure that is on them (Fletcher et al. 2010).

This study examines the vulnerability due to inundation of Kahului and Lahaina, Maui, using the SLR estimates by Vermeer and Rahmstorf (2009). Due to the uncertainty in their estimates, a scenario-building approach (NOAA 2001) is utilized where the +0.75 m estimate is used as a best-case SLR scenario, and the +1.9 m estimate is used as a worst-case SLR scenario. The purpose of this study is to use LiDAR DEMs to map low-lying lands vulnerable to SLR combined with spatial analysis to identify coastal habitats, roads, land and building values that are likely to experience adverse impacts.

2 Study area and data

2.1 Study area

The study area includes two communities with the most socioeconomic activity on Maui Island: Kahului and Lahaina (Fig. 1). Kahului is the largest community on the island with a Census 2010 population of nearly 26,000. The study area covering Kahului is ~8.9 km^2. Kahului is located on the north shore of a low-relief isthmus on a coastal plain between the dormant Haleakalā volcano to the east, and the extinct West Maui Volcano. Kahului is the industrial center of the island and the location of Kahului Harbor, Maui’s commercial deep-draft harbor; and Kahului Airport, Maui’s main airport that accommodates inter-island and mainland flights. Just inland to the Harbor sits the wetlands of Kanaha Pond, a designated National Natural Landmark and wildlife refuge for endangered Hawaiian bird species such as the ae‘o (Hawaiian stilt), and the ‘alae ke‘oke‘o (Hawaiian coot). Heavy vegetation surrounds Kanaha Pond and the shoreline just east of the wildlife refuge at Kanaha Beach Park.

Lahaina is an historic port town and largest community located on the shore of West Maui with a Census 2010 population of nearly 11,700. The study area covering Lahaina is ~4.9 km^2. As the second largest tourism destination of the Hawaiian Islands following Waikiki, visitors account for a much higher population around 40,000 during peak travel season. Lahaina’s shoreline consists of critical infrastructure such as the only highway that leads to Lahaina, the Hono a Pi‘ilani Highway (Route 30), coastal roads, and the Lahaina Harbor.

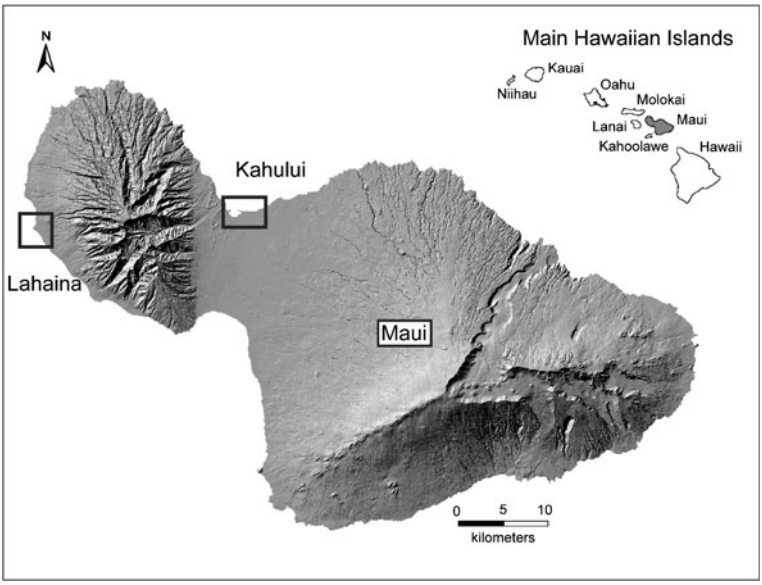

Fig. 1 Study areas of Kahului and Lahaina on Maui Island

2.2 Airborne LiDAR data

Two separate existing LiDAR datasets were used for Kahului and Lahaina, respectively. The data for Kahului were collected by the Joint Airborne LiDAR Bathymetry Technical Center of Expertise (JALBTCX) for the U.S. Army Corps of Engineers (USACE) in January through February of 2007 using the Compact Hydrographic Airborne Rapid Total Survey (CHARTS) system equipped with the Optech SHOALS-3000 sensor. The flight altitude varied from 300 to 1,200 m above ground level. The metadata reports the average laser point spacing as 1.3 m, and the vertical root mean square error (RMSE) as better than ±0.20 m. The Kahului data are called USACE LiDAR hereinafter. The data for Lahaina were collected by EarthData Aviation for the National Oceanic and Atmospheric Administration (NOAA) in March of 2005 during Mean Lower Low Water (MLLW) tides using the Leica Geosystems ALS-40. The flight altitude was ~800 m above mean ground level. The metadata reports the average laser point spacing as 2 m, the RMSE as ±0.162 m, and the vertical accuracy as ±0.318 m at the 95 % confidence level. The Lahaina data are called NOAA LiDAR hereinafter. Both USACE and NOAA LiDAR data were captured by discrete-return, scanning airborne laser altimeters with a pulse rate of 20,000 Hz.

Orthometric elevations were derived from the Geodetic Reference System of 1980 (GRS80) ellipsoid elevations using the National Geodetic Survey (NGS) GEOID03 model for USACE, and the NGS GEOID09 model for NOAA. These elevations were adjusted to the Local Tidal Datum of Mean Sea Level (MSL) and are in meters. However, it is unclear to which MSL tidal datum epoch the USACE and NOAA LiDAR are vertically referenced. The horizontal coordinates for the two data are relative to the North American Datum of 1983 (NAD83) and are in meters. The two data were received as classified ground returns in xyz format from the NOAA Coastal Services Center (CSC).

3 Methods

3.1 LiDAR data filtering and DEM generation

The quality of a LiDAR DEM is highly dependent on the average point spacing and the post-processing software used to filter the raw LiDAR 3-dimensional (3-D) point cloud, a set of points defined by xyz in a coordinate system. The data service providers for the USACE and NOAA LiDAR point data used proprietary procedures and software when filtering the LiDAR point cloud into classified ground returns. For this reason, an exploratory analysis of the USACE and NOAA ground returns was conducted to determine the effect of filtering methods on inundation analysis. DEMs of 2 m horizontal spatial resolution were generated from the two datasets using Toolbox for LiDAR Data Filtering and Forest Studies (Tiffs) software (Chen 2007). The 2 m cell size was chosen due to the average point spacing of the two data. The xyz files were also converted to the shapefile format so that the DEMs and LiDAR point shapefiles could be overlaid in 3-D using ESRI's ArcScene and visually compared with 2005 and 2007 aerial photos. This allowed for identification of any remaining vegetation or buildings that were not removed when the LiDAR point cloud was classified into ground and non-ground returns (e.g. vegetation and buildings).

Exploratory analysis of the NOAA ground returns overlaid with 2005 aerial photos demonstrated a lack of ground returns near buildings and vegetation. Since filtering the LiDAR point data is intended to remove vegetation and infrastructure, this is likely a cause of over-classification of the points as non-ground returns. This could not be further examined because the non-ground returns were not available for download from NOAA CSC to include in the exploratory analysis. It could not be determined how the filtering methods used for the NOAA data impact the DEM and inundation analysis for Lahaina.

Exploratory analysis of the USACE ground returns overlaid with 2007 aerial photos found vegetation along the coastline at Kanaha Beach Park and near Kanaha pond, which created topographic anomalies in the DEM. This is likely a cause of poor penetration of the LiDAR through thick canopy and misclassification of vegetation as ground returns. The Tiffs software uses an automatic grid-based filtering or morphological method (Chen et al. 2007), which was used to re-classify ground returns from the USACE data. This was done with caution to not over-classify vegetated areas that would leave a lower point density, such as in the NOAA data. After the points were re-classified, the ground returns were used to re-generate a refined 2 m USACE DEM.

3.2 Assessing vertical accuracy using tidal benchmarks

The standard for determining the quality of LiDAR data for the purpose of generating a DEM is to relate the data to a vertical datum (Maune 2007; Liu 2011). It is unclear whether the USACE and NOAA LiDAR are vertically referenced to the Local Tidal Datum of MSL for the recent 1983–2001 epoch. Therefore, this study used tidal benchmarks to assess the USACE LiDAR data and to determine if a calibration was needed. The USACE LiDAR was then used to determine if the NOAA LiDAR required calibration, due to the deficiency of tidal benchmarks in West Maui.

A particular order and class defined by the NGS classify the vertical accuracy of the tidal benchmarks, where more information on leveling can be found at http://www.ngs.noaa.gov/heightmod/Leveling/requirements.html. The tidal benchmarks 161 5680 A and C TIDAL are classified as third-order (the least accurate) and the seven remaining tidal benchmarks are classified as first-order, class I (most accurate). The tidal benchmark elevations were

compared with elevations derived from the USACE LiDAR data to calculate the mean difference, RMSE and the linear error ($L.E._Z$) at 95 % confidence. A standard t-test was used to inspect the difference between the tidal benchmark elevations and USACE LiDAR elevations, and the difference between the average elevations of the USACE and NOAA LiDAR point data in Northwest Maui where the two LiDAR datasets overlap to determine if a calibration was needed.

The LiDAR data filtering methods used may also affect the vertical accuracy assessment of the data because ground returns may have been misclassified (Liu 2011). The tidal benchmarks are located in flat and non-vegetated terrain, yet the LiDAR filtering process may have incorrectly classified non-ground returns as ground returns in the LiDAR point data covering the tidal benchmarks. In order to visualize the accuracy of the LiDAR point data, both the LiDAR point data and tidal benchmark point shapefiles downloaded at http://www.ngs.noaa.gov/ were examined together in 3-D using ESRI's ArcScene to visually determine that no misclassifications were made. The elevations of the 10 NOAA NGS tidal benchmarks were referenced to the horizontal datum of NAD83 and the vertical datum of Local Tidal Datum of MSL.

Methods used for the accuracy assessment of the LiDAR data were similar to those of Liu (2011). A subset of USACE LiDAR points within a 2 m radius of each tidal benchmark was selected, which was dependent on the average point spacing of the LiDAR point data. If there were no LiDAR point data within a 2 m radius of the tidal benchmark, then the tidal benchmark was excluded from analysis. Each subset of LiDAR point data was averaged to represent the LiDAR elevation at the location of the tidal benchmark. The tidal benchmark elevation was then compared with the LiDAR elevation. The difference between each tidal benchmark elevation and the LiDAR elevation was calculated along with the mean difference. The tidal benchmark elevation was also compared with the refined USACE DEM. The grid cell elevation located at the tidal benchmark was obtained by overlaying the two data in ESRI's ArcGIS. The difference between each tidal benchmark elevation and the grid cell elevation was calculated along with the mean difference.

The NOAA LiDAR data was calibrated using the USACE LiDAR data as the quality control because no tidal benchmarks are located in West Maui. To avoid horizontal errors that will increase the RMSE, the ASPRS (2004) recommends that a slope <20 % grade is considered when selecting quality control points. A stricter criterion was applied to find flat ground for calibration by choosing a ≤6 % slope in Northwest Maui where the USACE and NOAA LiDAR datasets overlapped. The ≤6 % slope was chosen because subsets were taken on roads such as the Hono a Pi'ilani Highway, and the U.S. Standards for Interstate Highways allow a maximum 6 % slope. The ≤6 % slope was determined by generating a 2 m DEM from the USACE LiDAR ground point data using Tiffs software. The slope function in ESRI's ArcGIS was used to transform the USACE LiDAR DEM to a new raster that defines the slope for each cell. The reclassify function in ESRI's ArcGIS was then used to reclassify the raster to find cells of ≤6 % slope.

A subset of the two overlapping LiDAR point datasets were selected in ten locations spread throughout Northwest Maui that were bounded by perimeters of basketball courts, tennis courts, roads and parking lots. Ten locations were chosen in Northwest Maui because ten tidal benchmarks were used for the USACE LiDAR analysis in Kahului. The USACE and NOAA sub-datasets were visualized in 3-D using ESRI's ArcScene to identify any misclassified ground points that needed to be removed from the analysis. Each subset of the two LiDAR point data was averaged for each location, and the USACE LiDAR elevation was compared with the NOAA LiDAR elevation. The difference between the USACE elevation and NOAA elevation was calculated along with the mean difference.

The RMSE was calculated for the USACE LiDAR using the equation from the ASPRS (2004):

$$\mathrm{RMSE} = \mathrm{Sqrt}\left[\left(\sum \left(Z_{\mathrm{data(i)}} - Z_{\mathrm{check(i)}}\right)^2\right)/n\right] \quad (1)$$

where $Z_{\mathrm{data(i)}}$ is the elevation of the USACE LiDAR, and $Z_{\mathrm{check(i)}}$ is the elevation of the tidal benchmark, and n is the number of tidal benchmarks used. The L.E.$_Z$ of ±0.318 m at 95 % confidence reported in the NOAA LiDAR metadata was considered because there are no tidal benchmarks located in West Maui to make an independent assessment. The L.E.$_Z$ at 95 % confidence was calculated for the USACE data, as recommended by the National Standard for Spatial Data Accuracy (FGDC 1998) and ASPRS (2004):

$$\mathrm{L.E.}_Z = 1.96 \times \mathrm{RMSE} \quad (2)$$

In the above equation, factoring the RMSE by 1.96 achieves greater probability where 95 % of the LiDAR vertical positions at these locations are in error to true ground vertical positions that will not exceed this accuracy value (FGDC 1998). Accordingly, the vertical accuracy of the USACE and NOAA data does not exceed the calculated L.E.$_Z$ at 95 % confidence, respectively.

3.3 Local tidal datum

For the conterminous U.S. and parts of Alaska, the current official vertical datum is the geodetic North American Vertical Datum of 1988 (NAVD88) used for deriving orthometric heights above or below a geoid model. Hawai‘i is an exception to this unified reference datum in that more traditional methods are used when defining its vertical datum, in which elevations are referred to Local Tidal Datum (NOAA 2008). This means that orthometric heights in Hawai‘i are considered to be above Local Tidal Datum of MSL. A certain phase of the tide defines a modeled elevation called a tidal datum (NOAA 2010), which is transferred inland to local tidal benchmarks using the method of differential leveling (NOAA 2001). The spatial distributions for the tidal benchmarks are in close approximation, with the furthest tidal benchmark at a distance of only ~650 m from the Kahului Harbor tide station (Fig. 2). Tidal datums are managed by NOAA National Oceanic Service (NOS) Center for Operational Oceanographic Products and Services (CO-OPS). CO-OPS tidal stations are located on U.S. Pacific and Atlantic coasts, the Gulf of Mexico, islands in the Atlantic and Pacific Oceans, Alaska and Hawai‘i.

Inundation mapping should be referenced to the tidal datum of Mean High Water (MHW) for the worst-case scenario (NOAA 2001). However, because Hawai‘i experiences semidiurnal tides, this study uses Mean Higher High Water (MHHW). MHHW is the average of the higher high water height observations of each tidal day at a control tide station, such as the Kahului Harbor tide station, over a 19-year National Tidal Datum Epoch (http://tidesandcurrents.noaa.gov/mhhw.html). Due to rising sea level, the National Tidal Datum Epoch was established for monitoring change in global sea level (NOAA 2009).

The current tidal epoch at the Kahului Harbor tide station on Maui Island is the tidal epoch of January 1983 to December 2001. The tidal datum of MHHW for this epoch is 1.422 m above the Station Datum, and the tidal datum of MSL for this epoch is 1.075 m above the Station Datum. Tidal datums are referenced to a fixed base established at an elevation below the water known as the Station Datum (http://tidesandcurrents.noaa.gov/).

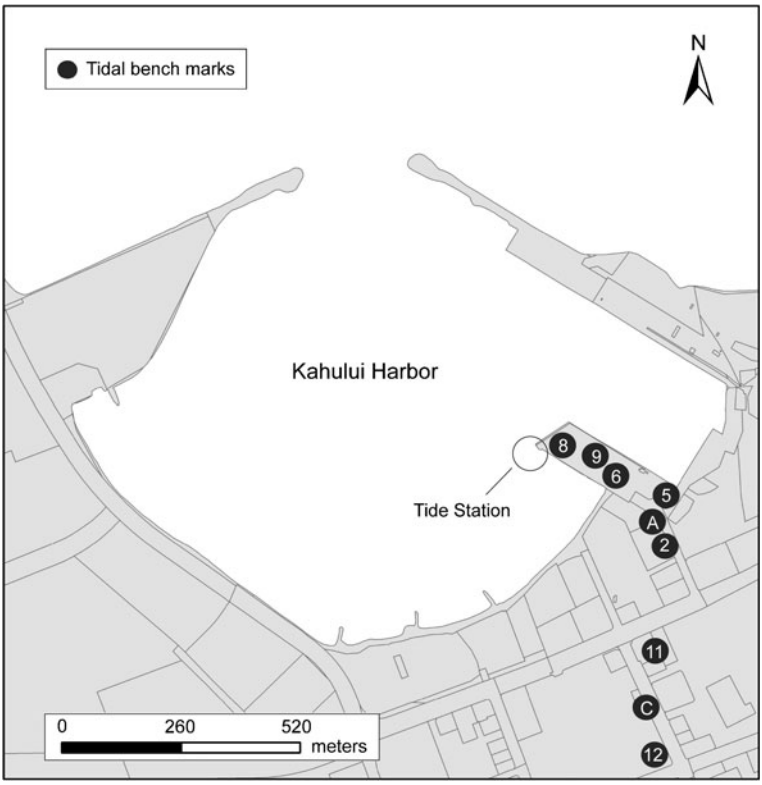

Fig. 2 The spatial distribution of the tidal benchmarks located at Kahului Harbor where the Local Tidal Datum of Mean Sea Level (MSL) is transferred inland

The difference between these two tidal datums (0.347 m) is considered in addition to each SLR scenario to assess the impacts of SLR at higher high tide.

3.4 Vulnerability assessment integrating LiDAR DEMs into GIS

The LiDAR DEMs were integrated into ESRI's ArcGIS to quantitatively assess the spatial distributions of areas subject to inundation on Kahului and Lahaina. The reclassify function in ESRI's ArcGIS was used to identify elevation values for each grid cell that lay below each of the given SLR scenarios from the LiDAR DEMs, in addition to the given SLR scenario $+L.E._Z$ at 95 % confidence (Gesch 2009). This identified each raster cell below the specified SLR scenario and the specified SLR scenario $+L.E._Z$ at 95 % confidence as "vulnerable". Vulnerable cells were separated into two groups based on hydrologic connectivity: the cells that are connected to an adjacent grid cell flooded or in open water (Poulter and Halpin 2008) are called Hydrologic Connected (HC); otherwise, they are called Hydrologic Disconnected (HD). For HC, we used the 8-side approach (Poulter and Halpin 2008; Henman and Poulter 2008; Gesch 2009; Marcy et al. 2011) (Fig. 3). NOAA, Digital Coast (2011) separately maps HD cells because the LiDAR DEMs lack an engineering grade hydrologic analysis of ditches and culverts that may cause inaccurately mapped areas, and HD areas may flood depending on how well the DEMs represent the area's hydraulics (Marcy et al. 2011). For these reasons, HD cells are included separately in our analysis because they represent vulnerability to high water

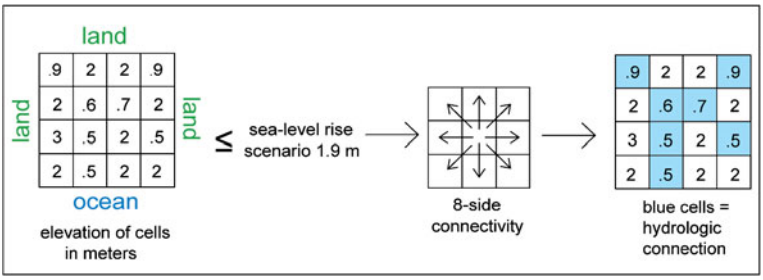

Fig. 3 The 8-side approach used to determine areas with hydrologic connection (HC) to the ocean

tables and poor drainage. Eight Geographic Information System (GIS) vulnerability layers were produced using the raster to polygon function in ESRI's ArcGIS, depending on whether we are considering 1) HC or HD areas, 2) best-case (+0.75 m) or worst-case (+1.9 m) SLR scenarios, and 3) with or without the vertical uncertainty $L.E._Z$ at 95 % confidence.

The intersect function in ESRI's ArcGIS was used to intersect vulnerable layers with GIS layers obtained from the Hawai'i Statewide GIS Program such as major and minor roads and land parcels. The total land area and length of roads impacted were calculated by taking the sum of the total area and length of roads within each of the vulnerability layers. The land and building value impacted within each parcel was assessed by multiplying the total land and building value within a parcel by the ratio of vulnerable area within the parcel to the total parcel area (Zhang et al. 2011). The total land and building value impacted within each of the vulnerability layers was then calculated by taking the sum of these values.

4 Results and discussion

4.1 Impacts of original vs. refined DEMs on inundation mapping

Poulter and Halpin (2008) suggested that LiDAR post-processing could influence inundation analysis. This study found that quantifying low-lying lands vulnerable to inundation due to SLR scenarios is liable to change because of filtering methods that classify the LiDAR point cloud into ground and non-ground returns. The filtering methods were most influential at the worst-case SLR scenario of +1.9 m and +1.9 m $+L.E._Z$ at 95 % confidence when compared to the best-case SLR scenario of +0.75 m and +0.75 m $+L.E._Z$ at 95 % confidence for hydrologically connected (HC) areas (Table 1). The topographic anomalies caused by interpolating vegetated areas misclassified as ground returns resulted in less area inundated along Kanaha Beach Park in the original USACE DEM at the worst-case SLR scenario of +1.9 m and +1.9 $+L.E._Z$ at 95 % confidence. Reclassifying the points located within vegetated areas as non-ground returns removed the topographic anomalies from the refined USACE DEM, thus causing more land area to be inundated at the worst-case SLR scenario of +1.9 m and +1.9 m $+L.E._Z$ at 95 % confidence. Since no more than ground returns were available from the data providers, another round of filtering may have reduced the commission errors of ground returns. Commission errors are when features such as vegetation are classified as ground-returns when they should not be classified as ground returns. Instead, these features should be classified as non-ground returns. However, another round of filtering cannot reduce the omission errors because only ground-returns were available from the data service provider. Although the difference in land area inundated between the original and refined

Table 1 Difference in land area inundated between the original and refined USACE DEM for Kahului, Maui. MHHW = Mean Higher High Water (1983–2001 epoch), L.E.$_Z$ 95 %=0.45 m, HC = hydrologically connected areas, and HD = hydrologically disconnected areas

	Original		Refined		Original		Refined		Original		Refined		Original		Refined	
	MHHW + 0.75 m		MHHW + 0.75 m		MHHW + 0.75 m + L.E.$_Z$		MHHW + 0.75 m + L.E.$_Z$		MHHW + 1.9 m		MHHW + 1.9 m		MHHW + 1.9 m + L.E.$_Z$		MHHW + 1.9 m + L.E.$_Z$	
Impacts	HC	HD	HC	HD	HC	HD	HC	HD	HC	HD	HC	HD	HC	HD	HC	HD
Land (km^2)	0.06	0.49	0.06	0.49	0.09	0.83	0.09	0.86	1.95	0.12	2.03	0.1	2.94	0.07	2.98	0.08

USACE DEM for the worst case SLR scenario of +1.9 m and +1.9 m +L.E.$_Z$ at 95 % confidence seems small (<5 %), the difference in impacts to land and building value is significant for the SLR scenario of +1.9 m (up to ~15 %, see Table 2).

4.2 Using tidal benchmarks to correct LiDAR elevations

The RMSE calculated for the USACE LiDAR point data and the refined USACE DEM were the same; 0.23 m (Table 3). The RMSE of 0.23 m was used in Eq. 2 for the USACE LiDAR to calculate a L.E.$_Z$ of ±0.45 m at 95 % confidence. The L.E.$_Z$ of ±0.318 m at 95 % confidence reported in the NOAA LiDAR metadata was considered. When the L.E.$_Z$ at 95 % confidence upper bound is added to the specified SLR scenario, additional elevation would be vulnerable (Figs. 4 and 5) given the vertical uncertainty of the LiDAR data (Gesch 2009).

From the original 10 tidal benchmarks used to define the Local Tidal Datum on Maui Island, one tidal benchmark was removed from analysis due to a lack of LiDAR points located within a 2 m radius. LiDAR point data within each of the remaining 9 tidal benchmarks ranged from 1–12 points (Table 3). Although the tidal benchmarks are located in a flat area, the LiDAR point elevation within a 2 m radius of each tidal benchmark ranges 0–0.16 m. The mean difference in elevation of the tidal benchmarks and LiDAR points was equivalent to the mean difference of the tidal benchmarks and the refined USACE DEM at 0.09 m. The average difference between the USACE LiDAR points and the tidal benchmarks is small (0.09 m) and not significant at the 0.05 levels (Table 3), meaning that no corrections had to be made to the refined USACE DEM.

Table 2 Difference in impacts to land and building value (over hydrologically connected areas) between the original and refined USACE DEM for Kahului, Maui. MHHW = Mean Higher High Water (1983–2001 epoch), and L.E.$_Z$ 95 %=0.45 m

	MHHW + 1.9 m		MHHW + 1.9 m + L.E.$_Z$	
Impacts	Original	Refined	Original	Refined
Land (km^2)	1.95	2.03	2.94	2.98
Land value ($)	194,268,694	214,183,202	356,048,216	369,017,038
Building value ($)	52,449,815	60,197,247	150,181,331	154,525,815

Table 3 Elevation differences between tidal benchmarks at the Kahului Harbor tide station, USACE LiDAR point data and refined USACE DEM. n = total number of LiDAR points, Z_{min} and Z_{max} = the minimum and maximum LiDAR point elevation, Z_{μ} represents the mean elevation of LiDAR points, Z_{DEM} = the refined USACE DEM elevation, Z_{BM} = the tidal benchmark elevation, Δ_{pts} = the elevation difference between the mean elevation of LiDAR points and the tidal benchmark (Z_{μ} - Z_{BM}), and Δ_{DEM} = the elevation difference between the refined USACE DEM and the tidal benchmark in meters (Z_{DEM} - Z_{BM}). RMSE means root mean square error

Tidal Benchmark	LiDAR points					Z_{DEM}	Z_{BM}	Δ_{pts}	Δ_{DEM}
	n	Z_{min}	Z_{max}	Z_{σ}	Z_{μ}				
161 5680 A	1	2.15	2.15	0.00	2.15	2.11	1.93	0.22	0.18
161 5680 C TIDAL	6	1.65	1.85	0.07	1.77	1.76	1.46	0.31	0.3
161 5680 TIDAL 11	9	2.02	2.11	0.03	2.05	2.06	2.11	−0.06	−0.05
161 5680 TIDAL 12	8	1.68	1.81	0.04	1.75	1.76	1.37	0.38	0.39
161 5680 TIDAL 2	12	2.15	2.23	0.03	2.19	2.2	2.50	−0.31	−0.3
161 5680 TIDAL 5	12	2.05	2.18	0.04	2.11	2.11	1.86	0.25	0.25
161 5680 TIDAL 6	3	2.58	2.61	0.02	2.59	2.58	2.41	0.18	0.17
161 5680 TIDAL 8	5	2.64	2.71	0.03	2.67	2.67	2.80	−0.13	−0.13
161 5680 TIDAL 9	7	2.50	2.66	0.06	2.56	2.54	2.58	−0.02	−0.04
Mean								0.09	0.09
RMSE								0.23	0.23

In Northwest Maui, the USACE LiDAR within the perimeters of basketball courts, tennis courts, roads and parking lots ranged from 64–288 points, while the NOAA LiDAR ranged from 15–72 points (Table 4). The lower point density of the NOAA LiDAR in Northwest Maui may confirm an over-classification of the data to remove infrastructure and vegetation. Another possible reason is that the two datasets originally have different point density. The NOAA average surface elevation was found to be significantly higher (mean difference of 0.38 m) than the USACE average surface elevation at the 0.05 levels (Table 4). This value was applied to correct the NOAA DEM.

This method of using the tidal benchmarks near a tide station to assess the vertical accuracy of the LiDAR proves useful for other low-lying communities considering SLR. For instance, a correction may be needed for the LiDAR because orthometric heights of the vertical datum to which the LiDAR is referenced may vary from local MSL; otherwise, unwarranted errors could be introduced into the SLR vulnerability maps (Poulter and Halpin 2008; Gesch 2009). This method provides an approach to address the many problems associated with lacking an established vertical datum, and may be particularly relevant for other islands.

For the purpose of SLR vulnerability mapping, problems to consider when working with tidal datums include that there are many variations such as MLLW, MSL, MHW, or MHHW. In addition, each variation of a tidal datum may refer to the current epoch of 1983–2001 or a superseded epoch such as 1960–1978. For the state of Hawai‘i, each tidal datum has unique values to each epoch where the superseded epoch is lower than the current epoch because global sea level has been slowly rising. As an example, the tidal datum of MSL for the 1960–1978 epoch on Maui Island is 1.039 m, and the tidal datum of MSL for the 1983–2001 epoch on Maui Island is 1.075 m. Another problem in lacking an

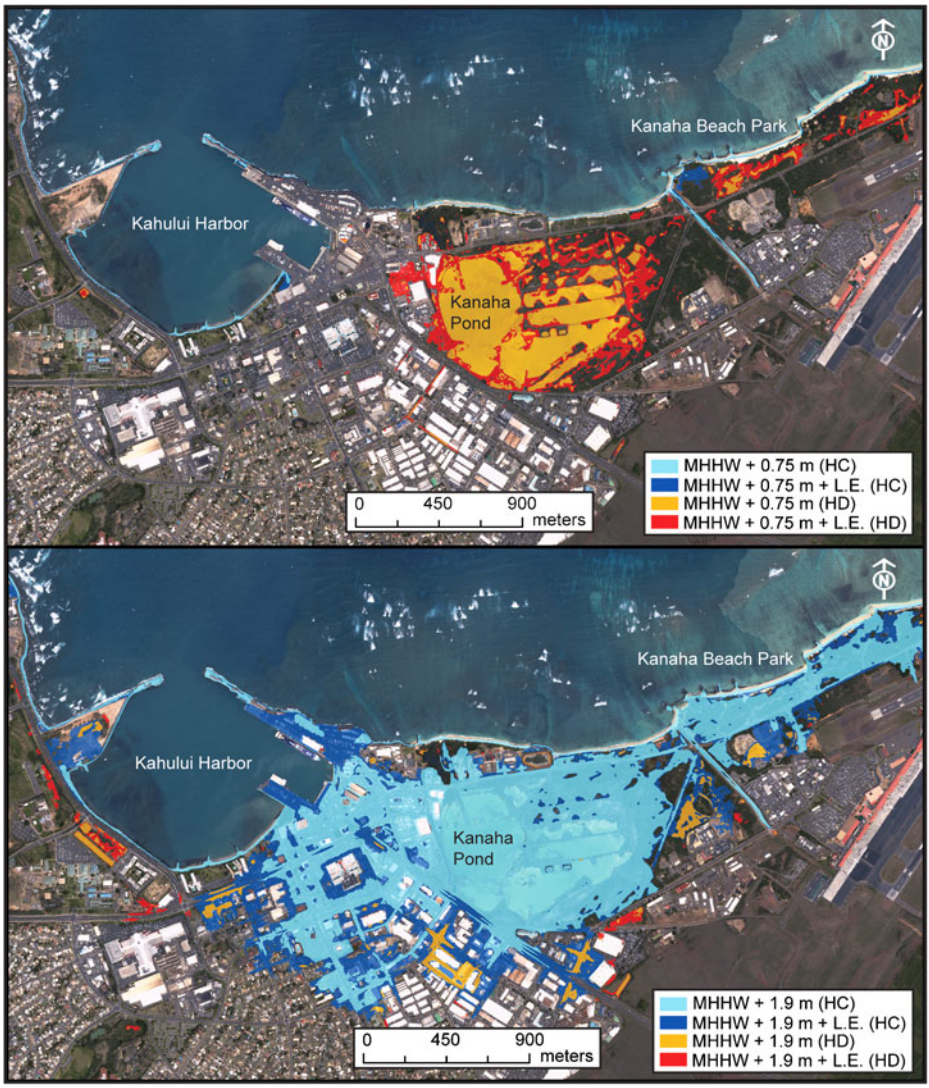

Fig. 4 SLR vulnerability maps of Kahului, Maui, highlighting lands vulnerable under the best-case SLR scenario of +0.75 m, and the worst-case SLR scenario of +1.9 m. The linear error (L.E.$_Z$) at 95 % confidence upper bound (0.45 m) estimates the vertical uncertainty of the elevation data at each SLR scenario contour. Vulnerable areas are separated by hydrologic connection (HC) and hydrologic disconnection (HD) from the ocean

established vertical datum is that each tidal datum varies from island to island. The LiDAR is vertically referenced to the Local Tidal Datum, yet there is no foundation to which island, which tidal datum, and which epoch is used. These inconsistencies could affect vertical accuracy assessment of the LiDAR and when applying different inundation scenarios, the accuracy of SLR vulnerability maps may be reduced. The NGS was consulted for this study to verify the lack of a vertical datum for Hawai‘i. This study calls for an established vertical datum among the Hawaiian Islands that

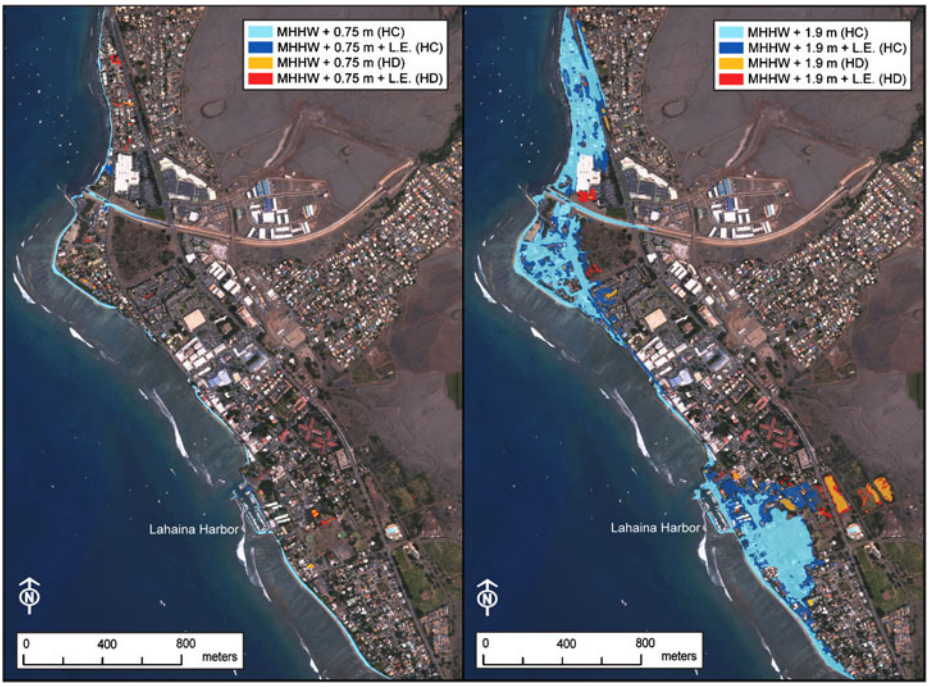

Fig. 5 SLR vulnerability maps of Lahaina, Maui, highlighting lands vulnerable under the best-case SLR scenario of +0.75 m, and the worst-case SLR scenario of +1.9 m. The linear error ($L.E._Z$) at 95 % confidence upper bound (0.318 m) estimates the vertical uncertainty of the elevation data at each SLR scenario contour. Vulnerable areas are separated by hydrologic connection (HC) and hydrologic disconnection (HD) from the ocean

proves important for other islands and low-lying coastal communities considering SLR so that consistent and accurate vulnerability maps can be produced.

Table 4 Analysis of ten locations with ≤6 % slope in Northwest Maui between the NOAA and USACE LiDAR point data. μ and σ are the mean and standard deviation of n NOAA or USACE LiDAR points, and Δ_μ = the difference between the mean NOAA and USACE LiDAR point elevations ($NOAA_\mu$ - $USACE_\mu$)

Description	Feature area (m^2)	Location (UTM, Zone 4, NAD 83)	Slope%	Z_{NOAA} (m)			Z_{USACE} (m)			Δ_μ (m)
				μ	σ	n	μ	σ	n	
Basketball court	122	744,014E, 2,324,251N	1-3	13.81	0.04	67	13.58	0.04	288	0.23
Parking lot	28	745,401E, 2,324,650N	1-6	72.16	0.06	15	71.76	0.10	80	0.40
Road 1	64	742,909E, 2,324,005N	4-6	32.13	0.13	34	31.91	0.16	260	0.22
Road 2	44	744,475E, 2,324,740N	3-6	18.00	0.12	40	17.59	0.10	126	0.41
Road 3	38	746,284E, 2,326,341N	3-6	57.06	0.09	27	56.47	0.10	117	0.59
Road 4	26	743,170E, 2,324,064N	3-5	50.97	0.07	19	50.65	0.09	68	0.32
Road 5	58	745,393E, 2,325,407N	6	21.91	0.20	51	21.45	0.20	67	0.46
Tennis court 1	43	743,491E, 2,324,279N	1-3	19.91	0.03	29	19.53	0.06	116	0.38
Tennis court 2	93	742,733E, 2,323,622N	1-3	13.53	0.04	72	13.15	0.03	112	0.38
Tennis court 3	38	745,081E, 2,324,552N	1-5	48.16	0.06	35	47.73	0.05	64	0.43
Mean										0.38

4.3 Quantitative assessment of vulnerability

Due to lower elevation on the north shore of Maui and larger study area, the inundation of total land area is greatest in Kahului when compared to Lahaina under each of the SLR scenarios (Tables 5 and 6). The overall impact to land value is greatest in Lahaina when compared to Kahului due to higher land value and greater tourist income associated with the high-value tourist beaches and active tourism industry of Lahaina. Most notable is the land and building value for Kahului is greater for HD than HC areas under the best-case SLR scenario of +0.75 m and +0.75 m +L.E.$_Z$ at 95 % confidence due to low relief areas just inland from the sea (Table 5). The impact to land value for Lahaina is consistently greater for HC than HD areas under each of the SLR scenarios and each of the SLR scenarios +L.E.$_Z$ at 95 % confidence (Table 6).

4.4 Vulnerability mapping and adaptation measures

Under the best-case SLR scenario of +0.75 m for HC areas (Fig. 4), the Kahului Harbor and shoreline will be inundated leading to beach erosion and beach loss. Under the best-case SLR scenario of +0.75 m plus L.E. at 95 % confidence for HC areas, more shoreline will be inundated at Kahului Harbor and inundation expands further inland near Kanaha Beach Park. Under the best-case SLR scenario of +0.75 m for HD areas, saltwater intrusion will significantly impact the freshwater Kanaha Pond Wildlife Sanctuary by threatening endangered bird species habitat. Under the best-case SLR scenario of +0.75 m +L.E.$_Z$ at 95 % confidence for HD areas, Kanaha Pond expands but does not open to the ocean. Expansion is likely driven by rise of the water table, which may be accompanied by saltwater intrusion through the ground. Research by Rotzoll et al. (2008) demonstrates that the coastal groundwater table responds to tide forcing and sits near to ground level in many locations on the Maui Coast. Rotzoll and El-Kadi (2008) also observed that wave-setup influences coastal groundwater tables as far inland as 5 km in central Maui. Vulnerability maps may allow for managers to identify and protect areas along with additional wildlife conservation efforts where the Sanctuary is likely to expand.

Under both the worst-case SLR scenario of +1.9 m and the worst-case SLR scenario of +1.9 m +L.E.$_Z$ at 95 % confidence for HC areas (Fig. 4), the commercial harbor will be adversely impacted by inundation. The harbor may experience changes in hydraulic characteristics such as swell and tide surge, inundation of facilities, and loss of operating hours. Coastal planners may be able to identify facilities that need to be relocated by moving further back from the coast in a planned retreat (Nicholls 2011).

Table 5 The impacts of sea-level rise on Kahului, Maui, under the best-case SLR scenario of +0.75 m, and the worst-case SLR scenario of +1.9 m. MHHW = Mean Higher High Water (1983–2001 epoch), L.E.$_Z$ 95 %=0.45 m, HC = hydrologically connected areas, and HD = hydrologically disconnected areas. * Land includes wetlands

Impacts	MHHW + 0.75 m		MHHW + 0.75 m + L.E.$_Z$		MHHW + 1.9 m		MHHW + 1.9 m + L.E.$_Z$	
	HC	HD	HC	HD	HC	HD	HC	HD
Land (km^2)*	0.06	0.49	0.09	0.86	2.03	0.1	2.98	0.08
Roads (km)	0.01	0	0.01	0.04	8.86	0.61	15.22	0.08
Land value ($)	3,329,879	14,030,458	6,205,975	32,104,620	214,183,202	13,590,455	369,017,038	5,896,246
Building value ($)	194 k	1,160,944	321 k	5,248,656	60,197,247	7,667,064	154,525,815	1,400,009

Table 6 The impacts of sea-level rise on Lahaina, Maui, under the best-case SLR scenario of +0.75 m, and the worst-case SLR scenario of +1.9 m. MHHW = Mean Higher High Water (1983–2001 epoch), $L.E._Z$ 95 %=0.318 m, HC = hydrologically connected areas, and HD = hydrologically disconnected areas

Impacts	MHHW + 0.75 m		MHHW + 0.75 m + $L.E._Z$		MHHW + 1.9 m		MHHW + 1.9 m + $L.E._Z$	
	HC	HD	HC	HD	HC	HD	HC	HD
Land (km^2)	0.04	0.002	0.05	0.007	0.34	0.03	0.52	0.03
Roads (km)	0.01	0	0.02	0.03	4.36	0.04	6.56	0.01
Land value ($)	50,780,093	2,546,572	77,750,071	5,338,930	323,559,652	6,250,192	489,084,020	7,705,300
Building value ($)	1,297,342	2,878,169	2,258,712	4,710,864	61,082,387	3,480,334	106,621,421	4,993,914

Under both the best-case SLR scenario of +0.75 m and the best-case SLR scenario of +0.75 m +$L.E._Z$ at 95 % confidence for HC areas (Fig. 5), the Lahaina Harbor and shoreline will be inundated leading to beach erosion and beach loss, which may impact visitors to the Island seeking prime beaches and recreational activities. Under both the worst-case SLR scenario of +1.9 m and the worst-case SLR scenario of +1.9 m +$L.E._Z$ at 95 % confidence for HC areas, the Hono a Pi'ilani Highway, coastal roads, residential neighborhoods, local businesses and resorts will be inundated and suffer drainage problems leading to adverse impacts to Lahaina's tourism industry. Under the worst-case SLR scenario of +1.9 m +$L.E._Z$ at 95 % confidence HD, these areas probably will not be flooded by waves but will materialize as areas lacking drainage where the ocean rises through the storm drain system and prevents runoff from draining, which will likely be accompanied by rise of the water table.

High-resolution SLR vulnerability maps (Figs. 4 and 5) are important to demonstrating low-lying coastal communities' vulnerability to SLR. Such maps highlight the critical need to take action in improving community resiliency to climate change and provide guidance on locations where vulnerability is high and underpin decision making for adaptation steps. SLR vulnerability mapping can help coastal planners consider the impacts of SLR by highlighting the lowest-lying lands and the critical infrastructure vulnerable to inundation and erosion. This allows for the proper adaptation measures to be taken, which may involve relocating coastal communities, housing, major and minor roads, local businesses, and ports located within each of the inundation zones. Relocating beachfront high-rise resorts further from the coast will be a difficult challenge. Decision makers could reduce vulnerability by decreasing development on coastal areas that are also considered high-risk, as featured on the SLR vulnerability maps. Using science-based setback rules, coastal planners in Maui County determine construction setbacks using erosion hazard maps (Genz et al. 2007). Following this example, steps could also include changing building codes to adopt revised base-flood elevations that incorporate SLR; retro-fitting transportation venues to avoid flooding, especially at traffic volume choke-points. High-resolution SLR vulnerability mapping is important to guiding any coastal community's adaptive strategies to climate change.

5 Conclusions

Using LiDAR for SLR vulnerability assessments presents many challenges. It is important to understand how LiDAR data are collected and post-processed in order to create reliable DEM products for inundation analysis, thus the significance of accurate and informative metadata. Questioning the quality of the LiDAR data may result in better understanding of how the data may influence inundation analysis. This study found that the post-processing

methods that filter the LiDAR point cloud into classified ground and non-ground returns used for DEM generation influence inundation analysis. Examining by visual inspection the quality of previous filtering results may identify problems where the commission errors of ground-returns identification can be reduced, which may improve SLR vulnerability assessments.

In the great majority of areas around the world lacking an established vertical datum, or with an outdated vertical datum, a relationship between high accuracy LiDAR and tide station references must be established. For Kahului Harbor on Maui Island, adjustments made from geoid heights to the Local Tidal Datum of MSL were successful. For future SLR vulnerability mapping, an established vertical datum would allow for more rigorous vertical accuracy assessments and merging of multiple LiDAR datasets located anywhere in the state.

If no adaptive strategies are taken, inundation due to SLR will lead to adverse socioeconomic impacts on Kahului and Lahaina. Under the best-case SLR scenario of +0.75 m for HC and HD areas combined, an impact to land and building value of $18.7 million is possible due to the inundation of 0.55 km^2 of area for Kahului, and an impact of $57.5 million is possible due to the inundation of 0.04 km^2 of area for Lahaina. As would be expected, adverse socioeconomic impacts to Kahului's commercial district and Lahaina's tourism industry are most profound for the worst-case SLR scenario of +1.9 m. Under this worst-case SLR scenario for HC and HD areas combined, an impact to land and building value of $296 million is possible due to the inundation of 2.13 km^2 of area for Kahului (which will also lead to wetland loss), and an impact of $394 million is possible due to the inundation of 0.37 km^2 of area for Lahaina. Our study demonstrates that there is a compelling need to improve community resiliency to SLR. Coastal planners in Hawai'i could require SLR vulnerability assessments as a first step toward building resiliency.

Improvements for future SLR vulnerability assessments may include up-to-date socioeconomic GIS data and mapping of the water table. For instance, GIS data of the spatial distributions of the Gross Domestic Product (GDP) by individual county, building footprints, population in each household, power stations, sewage, commuter density, traffic chokepoints, hospitals, evacuation routes, cultural sites, endangered species and imperiled ecosystems will serve useful for future SLR vulnerability assessments. Mapping of the water table and improved understanding of tidal and seasonal processes associated with vertical water table movement will improve vulnerability assessment of both HC and HD areas for the purpose of flood drainage and runoff engineering. Overall, SLR vulnerability mapping raises awareness of the potential impacts of SLR to the community, economy, and habitats of islands, and provides a valuable tool for coastal communities and policy makers considering adaptation strategies.

Acknowledgments We appreciate comments by three anonymous reviewers. Data were provided by the NOAA CSC, NGS, Hawai'i Statewide GIS Program, and DigitalGlobe. This study was funded by a grant from the U.S. Department of Interior Pacific Islands Climate Change Cooperative.

References

ASPRS (2004) ASPRS guidelines vertical accuracy reporting for LiDAR data, vol.1.0. http://www.asprs.org/a/society/committees/standards/standards_comm.html. Accessed 22 August 2011

CCSP (2009) Synthesis and assessment product 4.1: coastal sensitivity to sea-level rise: a focus on the Mid-Atlantic region. U.S. Climate Change Program, Washington, DC

Chen Q (2007) Airborne LiDAR data processing and information extraction. Photogramm Eng Rem Sens 73:109–112

Chen Q, Gong P, Baldocchi DD, Xie G (2007) Filtering airborne laser scanning data with morphological methods. Photogramm Eng Rem Sens 73:171–181
FGDC (1998) Geospatial positioning accuracy standards, Part 3. National Standard for Spatial Data Accuracy. FGDC-STD-007.3-1998. http://www.fgdc.gov/standards/projects/FGDC-standards-projects/accuracy/part3/index_html. Accessed 22 August 2011
Fletcher CH (2009) Sea level by the end of the 21st century: a review. Shore & Beach 77:4–12
Fletcher C, Boyd R, Grober-Dunsmore R, Neal WJ, Tice V (2010) Living on the shores of Hawai'i. University of Hawai'i Press, Honolulu
Genz AS, Fletcher CH, Dunn RA, Frazer LN, Rooney JJ (2007) The predictive accuracy of shoreline change rate methods and alongshore beach variation on Maui, Hawaii. J Coast Res 23:87–105. doi:10.2112/05-0521.1
Gesch DB (2009) Analysis of LiDAR elevation data for improved identification and delineation of lands vulnerable to sea-level rise. J Coast Res 53:49–58. doi:10.2112/S153-006.1
GOF (2011) The Global Oceans Forum report of activities 2010. www.globaloceans.org. Accessed 22 august 2011
Henman J, Poulter B (2008) Inundation of freshwater peatlands by sea level rise: Uncertainty and potential carbon cycle feedbacks. J Geophys Res 113:G01011. doi:10.1029/2006JG000395
IPCC (2007) Climate change 2007, the physical science basis. Cambridge University Press, Cambridge
Liu XY (2011) Accuracy assessment of LiDAR elevation data using survey marks. Surv Rev 43:80–93. doi:10.1179/003962611X12894696204704
Marcy D, Brooks W, Draganov K, Hadley B, Haynes C, Herold N, McCombs J, Pendleton M, Ryan S, Schmid K, Sutherland M, Waters K (2011) New mapping tool and techniques for visualizing sea level rise and coastal flooding impacts. In: Wallendorf LA, Jones C, Ewing L, Battalio B (eds) Proceedings of the 2011 Solutions to Coastal Disasters Conference, Anchorage, Alaska, June 26 to June 29, 2011., pp 474–90, Reston, VA: American Society of Civil Engineers. http://csc.noaa.gov/digitalcoast/tools/slrviewer/support.html#cite1. Accessed 17, March 2012
McLeod E, Poulter B, Hinkel J, Reyes E, Salm R (2010) Sea level-rise impact models and environmental conservation: a review of models and their applications. Ocean Coast Manage 53:507–517. doi:10.1016/j.ocecoaman.2010.06.009
Maune DF (2007) DEM User Requirements. In: Maune DF (ed) Digital elevation model technologies and applications: the DEM users manual, 2nd edn. American Society for Photogrammatry and Remote Sensing, Bethesda, pp 449–473
Nicholls RJ (2011) Planning for the impacts of sea level rise. Oceanography 24:144–157. doi:10.5670/oceanog.2011.34
NOAA (2001) Tidal datums and their applications. NOAA special publication NOS CO-OPS 1. NOAA National Ocean Service, Silver Spring
NOAA (2008) Topographic and bathymetric data considerations: datums, datum conversion techniques, and data integration. Technical Report NOAA/CSC/20718-PUB. National Oceanic and Atmospheric Administration, Charleston, SC
NOAA (2009) Sea level variations of the United States 1854–2006. Technical Report NOS CO- OPS 053. NOAA National Ocean Service, Silver Spring
NOAA (2010) Technical considerations for use of geospatial data in sea level change mapping and assessment. NOAA NOS Technical Report. NOAA National Ocean Service, Silver Spring
NOAA (2011) Digital Coast, NOAA Coastal Services Center. http://csc.noaa.gov/digitalcoast/tools/slrviewer/support.html#cite1. Accessed 17, March 2012
Poulter B, Halpin PN (2008) Raster modeling of coastal flooding from sea-level rise. Int J Geogr Inf Sci 22:167–182. doi:10.1080/13658810701371858
Rotzoll K, El-Kadi AL (2008) Estimating hydraulic properties of coastal aquifers using wave setup. J Hydrol 353:201–213. doi:10.1016/j.jhydrol.2008.02.005
Rotzoll K, El-Kadi AL, Gingerich SB (2008) Analysis of an unconfined aquifer subject to asynchronous dual-tide propagation. Ground Water 46:239–250. doi:10.1111/j.1745-6584.2007.00412.x
US Census Bureau (2011) The 2011 statistical abstract of the United States. US Census Bureau. Washington, DC. http://www.census.gov/compendia/statab/. Accessed 22 August 2011
Vermeer M, Rahmstorf S (2009) Global sea level linked to global temperature. Proc Natl Acad Sci 106:21527–21532. doi:10.1073/pnas/.0907769106
Wu SY, Yarnal B, Fisher A (2002) Vulnerability of coastal communities to sea-level rise: a case study of Cape May County, New Jersey, USA. Clim Res 22:255–270
Zhang K (2011) Analysis of non-linear inundation from sea-level rise using LiDAR data: a case study for South Florida. Clim Change 106:537–565. doi:10.1007/s10584-010-9987-2
Zhang K, Dittmar J, Ross M, Bergh C (2011) Assessment of sea level rise impacts on human population and real property in the Florida Keys. Clim Change 107:129–146. doi:10.1007/s10584-011-0080-2